coatings

MDPI

Review

Strategies of Anode Materials Design towards Improved Photoelectrochemical Water Splitting Efficiency

Jun Hu [1], Shuo Zhao [1], Xin Zhao [2,*] and Zhong Chen [2,*]

[1] School of Chemical Engineering, Northwest University, Xi'an 710069, China; hujun@nwu.edu.cn (J.H.); zhao981017@foxmail.com (S.Z.)
[2] School of Materials Science and Engineering, Nanyang Technological University, 50 Nanyang Avenue, Singapore 639798, Singapore
* Correspondence: xinzhao@ntu.edu.sg (X.Z.); ASZChen@ntu.edu.sg (Z.C.); Tel.: +65-6790-4256 (Z.C.)

Received: 4 April 2019; Accepted: 6 May 2019; Published: 9 May 2019

Abstract: This review presents the latest processes for designing anode materials to improve the efficiency of water photolysis. Based on different contributions towards the solar-to-hydrogen efficiency, we mainly review the strategies to enhance the light absorption, facilitate the charge separation, and enhance the surface charge injection. Although great achievements have been obtained, the challenges faced in the development of anode materials for solar energy to make water splitting remain significant. In this review, the major challenges to improve the conversion efficiency of photoelectrochemical water splitting reactions are presented. We hope that this review helps researchers in or coming to the field to better appreciate the state-of-the-art, and to make a better choice when they embark on new research in photocatalytic water splitting.

Keywords: photoelectrochemical; anode materials; surface; water splitting

1. Introduction

Nowadays, it is becoming the world's biggest challenge to meet the increasing energy demand by developing new sustainable substitution energy and reducing carbon dioxide emission. Overall, water splitting using sunlight is identified as a promising technology for production of renewable fuels and chemicals without causing environmental pollution.

In a photoelectrochemical cell for solar water-splitting, there are three main elements; namely, an anode, a cathode, and an electrolyte. At the anode, the oxygen evolution reaction (OER) will happen, while through the hydrogen evolution reaction (HER), hydrogen forms at the cathode, as shown in reactions R1 and R2 [1].

$$\mathrm{R1:}\ 2H_2O(l) \rightarrow 4e^- + 4H^+ + O_2(g) \quad (1)$$

$$\mathrm{R2:}\ 4H^+(aq) + 4e^- \rightarrow 2H_2 \quad (2)$$

The two half-reactions constitute the overall water splitting process ($2H_2O \rightarrow 2H_2 + O_2$), with the thermodynamic threshold energy E_0 = 1.23 eV. Although both reactions are important for the overall water splitting efficiency, the process is mainly hindered by the hypokinetic four-electron water oxidation. Based on electron transfer process, OER can be divided into four reaction paths with 1.23 eV in the surface site (denoted by the * symbol) of anode materials for thermodynamic threshold energy, as shown in reactions R3 to R6 [2].

$$\mathrm{R3:}\ H_2O + * \leftrightarrow OH^* + H^+ + e^- \quad (3)$$

$$R4: \ OH^* \leftrightarrow O^* + H^+ + e^- \quad (4)$$

$$R5: O^* + H_2O \leftrightarrow OOH^* + H^+ + e^- \quad (5)$$

$$R6: \ OOH^* \leftrightarrow O_2 + H^+ + e^- \quad (6)$$

After the Honda–Fujishima effect was discovered in the early 1970s [3], intensive studies were carried out for photoelectrochemical (PEC) water splitting on semiconducting materials. The semiconducting anode materials will greatly determine the efficiency of absorbing light, suitable over-potential, and stability. It is challenging to develop efficient new anode materials or improve the ability of existing anode materials. Consequently, extensive efforts were implemented to improve the efficiency of anode materials; for example, TiO_2, α-Fe_2O_3, WO_3, and $BiVO_4$ [4]. However, there is still lack of cheap and stable photoanode materials with sufficient efficiency for water oxidation. Although significant progress has been made by developing new materials, nanostructures, and other novel concepts over the past decades, efficiencies are still below our expectations. Therefore, to assist future development, we wish to summarize the strategies to develop anode materials for improved efficiency in PEC water splitting in a concise manner. It is up to the readers to decide how different strategies could be applied in their specific applications, or to apply them synergistically in some situations.

The solar-to-hydrogen (STH) efficiency is an important metric for benchmarking and performance evaluation. The STH for a PEC system constructed by photoelectrodes can be expressed by [5]:

$$\text{STH} = \frac{J_P \times 1.23}{I_0} \times 100\% \quad (7)$$

where J_P is the photocurrent observed from the experiment, I_0 is the power intensity of the sunlight. The number 1.23 in the equation is the approximated value of the threshold energy for water splitting which requires the bandgap energy of any possible photoanode lager than 1.23 eV. For a photoelectrode, J_P is determined by the photogeneration absorption efficiency (η_{abs}), the product of the injection efficiency (η_{sep}), and the injection efficiency (η_{inj}) of the photogenerated carrier to the reactant [6], which can be described by:

$$J_P = J_0 \times \eta_{abs} \times \eta_{sep} \times \eta_{inj} \quad (8)$$

where J_0 is the theoretical photocurrent when 100% of the photons in the solar spectrum with energies exceeding the bandgap are absorbed and converted. Theoretical STH and solar photocurrent of a photoelectrode under AM 1.5 G irradiation (100 mW·cm^{-2}) are displayed in Figure 1 [6].

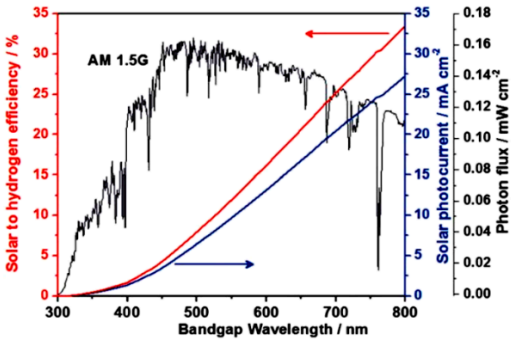

Figure 1. Dependence of theoretical solar-to-hydrogen (STH) efficiency and solar photocurrent density of photoelectrodes on their bandgap absorption edges. Reprinted with permission from ref. [5]. Copyright 2013. The Royal Society of Chemistry.

Thus, to achieve efficient PEC water splitting, several key criteria must be met, as shown in Figure 2: (1) wide range of light absorption of a material that can utilize more energy from sunlight; (2) effective generation of the charges and their transportation from the internal electrode to the photoelectric surface; (3) fast reaction of photogenerated carriers on the surface. Therefore, we will summarize recent progress of improving those efficiencies separately.

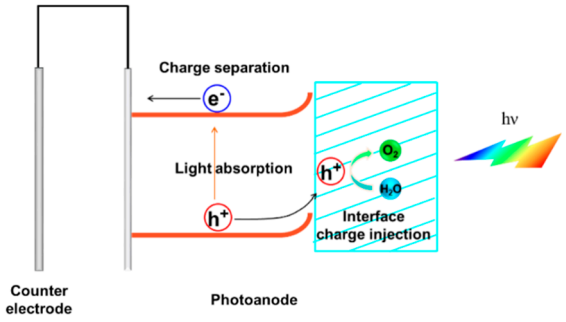

Figure 2. Schematic illustration of the three efficiencies of photoelectrochemical (PEC) water splitting for enhancing performance.

In this review, we summarize recent progress in the development of anode materials for photoelectrochemical water splitting, which are mainly based on our research work. This is carried out through a review of the strategies to enhance the light absorption, facilitate the charge separation, and enhance the surface charge injection. Finally, we share our critical views on the remaining challenges in this field.

2. Strategies to Enhance the Light Absorption

Generally, light absorption of a photoelectrode depends on its bandgap. For a known photoelectrode with a fixed bandgap, the film thickness and structure would affect its light absorption efficiency. Some reported strategies used to enhance the light absorption are summarized below.

2.1. Nanostructure Formation

Nanostructure is a good way to capture the scattered light if the light is not absorbed immediately after it reaches the surface. Nanostructure formation is a well-known strategy for silicon solar cells to reduce reflection loss and increase the energy conversion efficiency [7]. Similarly, nanostructure construction is proven effective in improving the light capture in PEC electrodes [8]. It has been reported that multiple light scattering in engineered tapered nanostructures enhances light absorption. (Figure 3) [9]. With a nanoporous Mo:$BiVO_4$ layer on the engineering conical nanophotonic structure combined with a solar cell, a STH efficiency of 6.2% was realized. Zhou et al. reported a hierarchical $BiVO_4$ photoelectrode, which consists of small nanoparticles and voids, could induce efficient light harvesting due to multiple light scattering [6]. Kim reported high-efficiency light absorption of GaN truncated nanocones. The truncated nanocones can trap the light within the nanostructure; thus, light loss, which is caused by surface reflection, is reduced. The TiO_2 solar cell prepared by using a 1D nanowire array can have a light conversion efficiency of up to 5.02%, which is much higher than that of a simple TiO_2 powder [10].

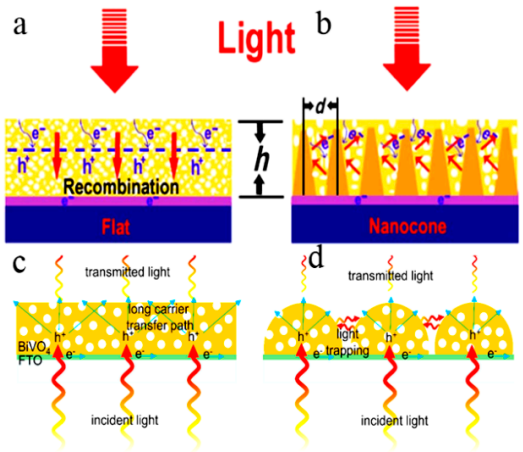

Figure 3. Optical absorption and electron transport on nanoporous $BiVO_4$ with (**a**) the flat substrate and (**b**) the conductive nanocone substrate. Reprinted with permission from ref. [9]. Copyright 2016. Science. (**c**) flat $BiVO_4$ film and (**d**) hierarchical $BiVO_4$ nanostructured film. Reprinted with permission from ref. [10]. Copyright 2008. American Chemical Society.

2.2. Band Engineering

To reduce the band gap of semiconductors, one commonly adopted and promising strategy is to add a foreign element (doping). Doping of foreign elements may include adding cation(s), anion(s), or adding cation(s) and anion(s) at same time.

Addition of cations usually induces a shallow valence band in the wide band gap through the hybrid valence orbital [11]. In metal oxide photocatalysts, incorporation of metal ions will introduce a donor level by hybridizing the O 2*p* valence orbitals with a metal ion having high-lying valence orbitals, such as Bi(III), Ag(I), Sn(II), Pb(II), or Cu(I). The crystal structure and the amount of metal incorporated greatly affect the contribution of the valence band. For example, in a MoO_3 electrode, Li^+, Na^+, and Mg^{2+} can greatly reduce the gap of the band [12,13]. Thus, modulating the band structure by cation doping is considered to be effective at the atomic level.

Anion doping has been employed to shift the absorption edge from the UV to the visible region; indeed, it is one of the strategies to enhance the light absorption. A lot of attention has been paid to nonmetal doping into TiO_2 to tune the light absorption, such as N doping as well as C, F, S, B doping [14]. For example, N and B doping greatly expands the light absorption to 700 nm [15]. Also, O incorporation in MoS_2 is able to improve the hybridization between Mo *d*-orbital and S *p*-orbital, resulting in a much smaller band gap [16]. Similarly, replacement of O by N in Ta_2O_5 induces a narrowed bandgap; for example, it was observed that the absorption was extended from 320 to 500 nm by N-doping (Figure 4) [17]. Simultaneously adding cations and anions can greatly change the band structure for enhancing the light absorption; e.g., the band gap of GaN is about 3.4 eV and the band gap of ZnO is 3.2 eV (Figure 5). However, the solid solution of GaN and ZnO narrowed the band gap to around 2.58 eV with visible light response [18]. This strategy provides us with a powerful method for adjusting the bandgap of photoelectrode materials through band engineering.

Another strategy for enlarging the light absorption is by intrinsic doping, such as introducing oxygen vacancy in oxides. The typical example is black TiO_2, in which lots of Ti^{3+} species are generated accompanied with the oxygen vacancy, being self-doping [19,20]. Doping and presence of lattice vacancies introduce midgap states which form the band tails and narrow the band gap. The light absorption of TiO_2 was enlarged to around 1000 nm from the 400 nm of white TiO_2. However, it is noted that the enlarged light absorption has little contribution to the enhanced performance, because the there is little visible light response for the black TiO_2 (Figure 6) [21]. The enhanced performance is possibly from the better conductivity.

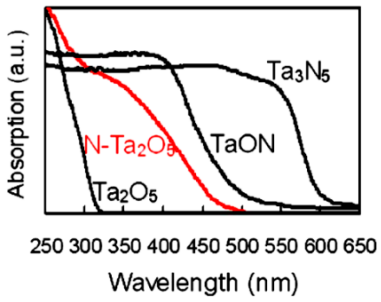

Figure 4. Diffuse reflectance absorption spectrum of N-Ta_2O_5 power (8.9 at. % N), nondoped Ta_2O_5, TaON, and Ta_3N_5 in the ultraviolet and visible light region. Reprinted with permission from ref. [17]. Copyright 2018. American Institute of Physics.

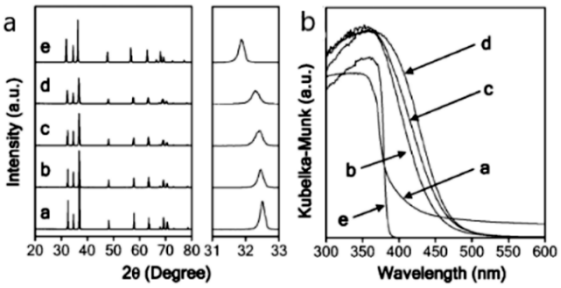

Figure 5. (**a**) Power X-ray diffraction pattern and (**b**) ultraviolet light visible diffuse reflectance spectra: a, b, c, d, e stand for GaN (ref), GaN:ZnO (Zn 3.4 at. %), GaN:ZnO (Zn 6.4 at. %), GaN:ZnO (Zn 13.3 at. %), and ZnO. Reprinted with permission from ref. [18]. Copyright 2018. American Chemical Society.

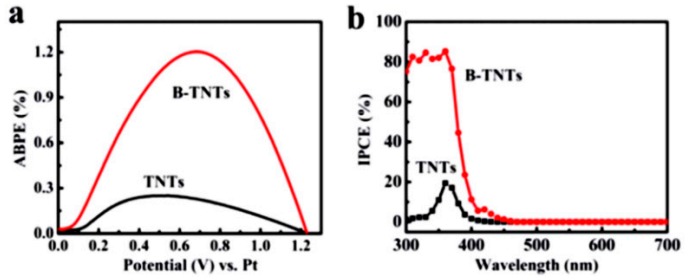

Figure 6. (**a**) Applied bias photon-to-current efficiency (ABPE) of the TiO_2 nanotubes (TNTs) and black titania nanotube (B-TNTs) as a function of applied potential; (**b**) incident-photon-to-current-conversion efficiency (IPCE) spectra in the region of 300–700 nm at 0.23 V vs. Ag/AgCl. Reprinted with permission from ref. [21]. Copyright 2014. The Royal Society of Chemistry.

2.3. Dual Absorber

Wang et al. reported extraordinary PEC performance by using dual $BiVO_4$ photoanodes made of two $BiVO_4$ which has the same transparency (Figure 7) [22]. The second electrode can use the transmitted light unabsorbed by the first electrode. It was found that the enhanced performance was mainly because of the higher light utilization rate in the airway scope of band edge (400–520 nm). A similar strategy was employed by Kim et al. with a different absorber; $BiVO_4$ in the front, and Fe_2O_3 behind $BiVO_4$ (Figure 8) [23]. This can further utilize the solar light, because Fe_2O_3 has a smaller bandgap than $BiVO_4$; thus, the transmitted light can be utilized by Fe_2O_3. This has increased the efficiency of hydrogen conversion to 7.7%. Wang et al. reported PEC water splitting using a hematite/Si nanowire dual-absorber system, which yielded a lower onset potential [24]. In their work, hematite was coated on the surface of Si nanowire, and the transmitted light through hematite was utilized by Si. The generated electrons of hematite combine with the holes generated on Si. Thus,

holes generated on hematite are used for water oxidation, and at the same time, electrons generated on Si are used for reduction reaction. The match of the band edge positions of the two absorbers is important. A double absorber series battery was reported by Sivula et al., in which the light transmitted through the photoelectrode material is utilized by the dye-sensitized solar cells (DSSC) that provides the bias needed by the photoelectrode [25]. This concept is very useful in tandem PEC cells, which do not need additional bias and can increase the solar conversion efficiency. Besides, Chang and Ye also added Co_3O_4 and carbon quantum dot (CQDs) components on the surface of $BiVO_4$ to enlarger light absorption range [26,27]. For instance, CQDs decorated $BiVO_4$ photoanode cocatalyzed by a bi-layered Ni-FeOOH oxygen evolution catalyst have obtained an outstanding photocurrent density of 5.99 $mA{\cdot}cm^{-2}$ at 1.23 V vs. reversible hydrogen electrode (RHE) with an enlarged light absorption range. Noble metal nanoparticles can also enhance the absorption light scattering/trapping, such as Au nanoparticles coated $BiVO_4$ and hematite [28,29]. However, the plasmonic effect also involves direct electron transfer mechanism (DET) and plasmon induced resonance electron transfer (PIRET) to enhance the performance except the light absorption. Currently, the full understanding of the involved physical mechanisms remains elusive, and requires more work to be clarifies [30].

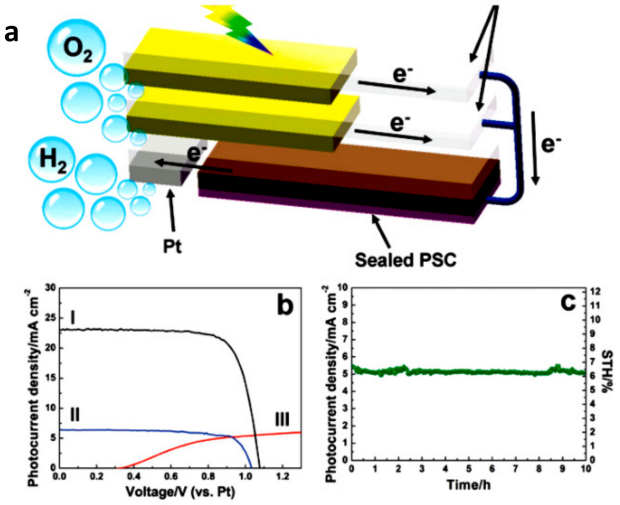

Figure 7. (**a**) The $BiVO_4$-FeOOH/NiOOH dual photoanodes coupled with s sealed perovskite solar cell; (**b**) I: *J*–*V* curve of perovskite solar cell, II: *J*–*V* curve of perovskite solar cell behind the BVO-FeOOH/NiOOH dual photoanodes, III: *J*–*V* curve of BVO-FeOOH/NiOOH under AM 1.5 G illumination; (**c**) Stability of unassisted water splitting (0 V vs. the counter electrode Pt). Reprinted with permission from ref. [22]. Copyright 2018. Wiley.

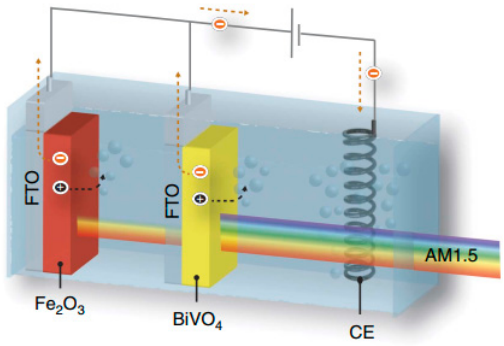

Figure 8. Wavelength-selective solar light absorption by hetero-type dual photoanode. Reprinted with permission from ref. [23]. Copyright 2018. Nature.

3. Strategies to Improve the Charge Separation

3.1. Doping

Doping is proved to be an effective way to improve the conductivity of semiconducting compounds and thus increase the charge separation efficiency [5]. Zhao et al. reported that extrinsic Ti doping and oxygen vacancy generation (intrinsic doping) have greatly enhanced the PEC performance of hematite (Figure 9) [31]. In another example, incorporation of Mo^{6+} into a partial site of V^{5+} in $BiVO_4$ not only has changed the crystal symmetry of $BiVO_4$ and introduced some polarons, but also provided more free carriers (electrons) which facilitate the charge transport [32,33].

Exploration of new materials with suitable band position and narrow bandgap for water splitting is still a vital issue. Since doping is proven as an effective method to ameliorate the efficiency through improved conductivity, this method is usually combined with the design and synthesis of new PEC electrode materials. Recently, the performance of a new promising material, Zn_2FeO_4, for PEC water splitting was improved by Ti doping (Figure 10) [34]. Lumley et al. reported that the performance of $Cu_{11}V_6O_{26}$ was enhanced after doping by Mo or W [35]. Jo et al. found the 0.5% PO_4-doped $BiVO_4$ can lower the charge transfer resistance of $BiVO_4$ remarkably, about 30 times higher than that of $BiVO_4$ before doping [36].

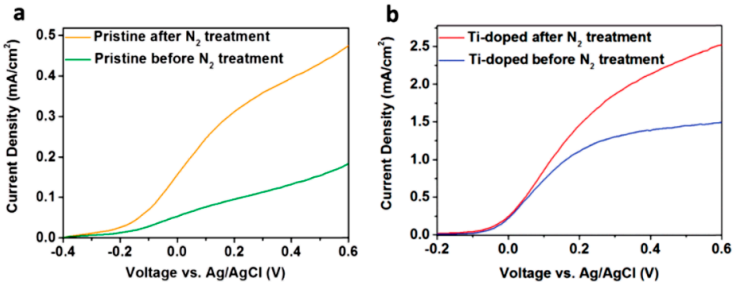

Figure 9. The photocurrents of (**a**) pristine and (**b**) Ti-doped hematite before and after N_2 treatment under AM 1.5 G solar simulator illumination. The N_2 treatment is carried out in nitrogen gas at 600 °C for 2 h. Reprinted with permission from ref. [31]. Copyright 2017. The Royal Society of Chemistry.

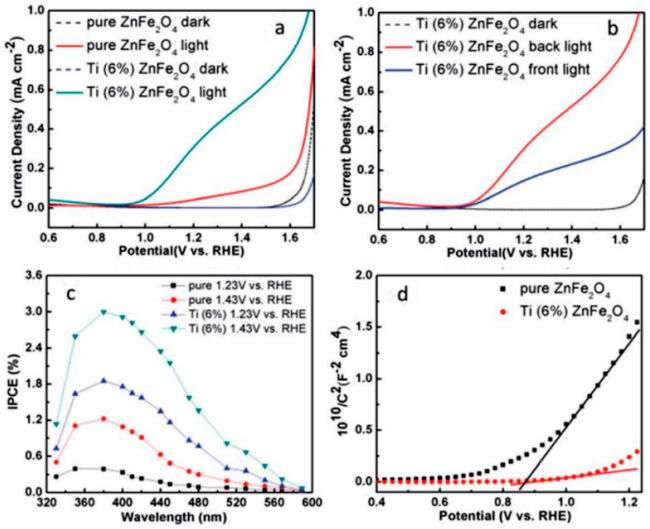

Figure 10. The photocurrents of (**a**) $ZnFe_2O_4$ photoanodes and Ti-doped $ZnFe_2O_4$ photoanodes in 1 M NaOH aqueous solution under AM 1.5 G illumination (100 mW·cm^{-2}); (**c**) IPCE spectrum of Ti-doped $ZnFe_2O_4$ and pure $ZnFe_2O_4$ in range from 330 to 589 nm at different applied potential; (**d**) Mott–Schottky plots of pure Ti-doped $ZnFe_2O_4$ and $ZnFe_2O_4$ photoanodes in 1 M NaOH, the AC amplitude is 5 mV and the frequency is 1000 Hz. Reprinted with permission from ref. [34]. Copyright 2018. American Chemical Society.

One special doping is gradient doping, which means that the dopant concentration varies from surface to the bulk. In such a case, the band bending not only occurs on the surface, but also in the bulk, which provides an electric field throughout the bulk material. It is easier for the carriers to separate and transport to the surface in a gradient electrode. Yang et al. investigated how gradient doping affects a GaAs photocathode and found that both the escape probability and the diffusion length increased when compared with uniform doping [37]. Abdi et al. synthesized a doped W gradually decreased $BiVO_4$ from 1% to 0% between the interface of the FTO/semiconductor and semiconductor/electrolyte (Figure 11) [38]. Based on their experiment, the efficiency of charge separation increases to ~60%, while the efficiency of charge separation is ~38% for equally doped $BiVO_4$ (Figure 12).

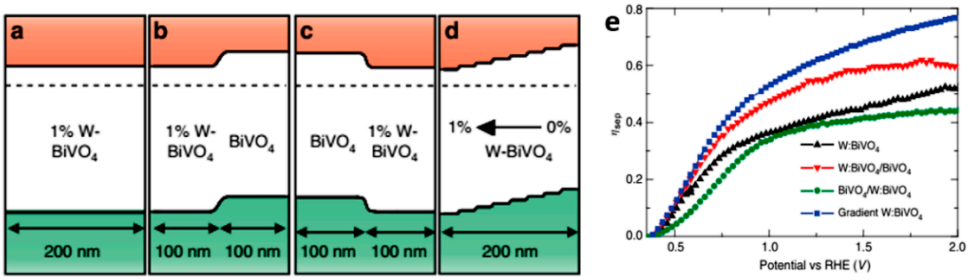

Figure 11. (**a**) 1% W-doped $BiVO_4$; (**b**) W:$BiVO_4$ homojunction; (**c**) W:$BiVO_4$ reverse homojunction; and (**d**) gradient-doped W:$BiVO_4$; (**e**) Carrier-separation efficiency (η_{sep}) in different applied potential for 1% W-doped $BiVO_4$ (black triangle), W:$BiVO_4$ homojunction (red inverted triangle), W:$BiVO_4$ reverse homojunction (green circle), and gradient-doped W:$BiVO_4$ (blue square). Reprinted with permission from ref. [38]. Copyright 2018. Nature.

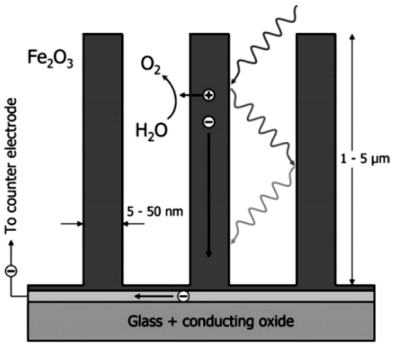

Figure 12. Illustration of the morphology of an α-Fe_2O_3 photo-anode for water splitting. The small diameter of nanowires ensures short hole diffusion path lengths. Reprinted with permission from ref. [39]. Copyright 2008. The Royal Society of Chemistry.

3.2. Nanostructure to Shorten the Diffusion Length

Besides conductivity improvement, the minority carrier's diffusivity is another key factor influencing the charge separation efficiency. Nanostructure provides a shorter diffusion distance for the minority carrier; therefore, it has been widely applied to improve the charge separation as shown in Figure 12 [39]. Kim et al. found nanoporous morphology of $BiVO_4$ can effectively suppress recombination, which yields an electron-hole separation efficiency as high as 90% at 1.23 V vs. RHE [40]. Zhao et al. also found enhancement of the performance by nanostructure compared with dense structure (Figure 13) and proved that the main contribution of the observed enhancement is the improved charge separation efficiency, which is caused by the easy diffusion of minority carriers to the interface [41]. Zhu et al. reported a nanorod-structured $ZnFe_2O_4$ with a new benchmark solar photocurrent of 1.0 mA·cm^{-2} at 1.23 V and 1.7 mA·cm^{-2} at 1.6 V vs. RHE (Figure 14) [42]. In general, if the average particle diameter of the nanopores is shorter than holes diffusion length, carrier recombination in bulk can be effectively inhibited. Table 1 shows holes diffusion length of some typical materials for OER.

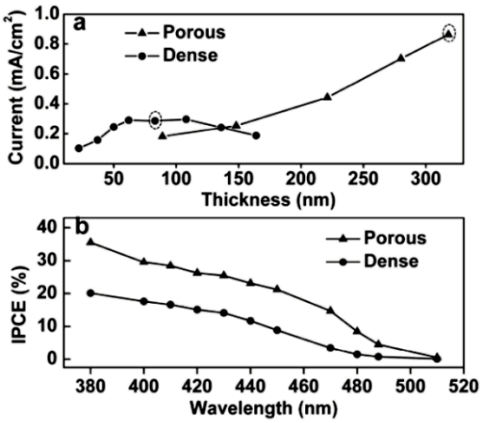

Figure 13. (**a**) The photocurrent at 1.23 V RHE of the porous and the dense Mo doped $BiVO_4$ films with different thickness in 0.5 M Na_2SO_4 aqueous solution under front (electrolyte-$BiVO_4$ surface side) illumination with a 500 W Xe lamp equipped with a 420 nm cut-off filter at a scan rate of 30 $mV{\cdot}s^{-1}$; (**b**) IPCE at 1.23 V RHE of the porous and the dense $BiVO_4$ films in 0.5 M Na_2SO_4 aqueous solution under front illumination. Reprinted with permission from [41]. Copyright 2018. Wiley.

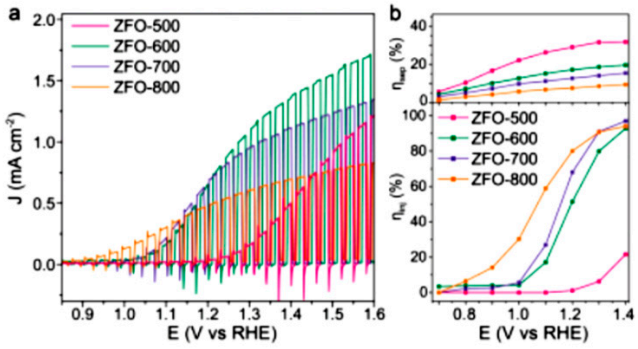

Figure 14. The performance of $ZnFe_2O_4$ (ZFO) photoanodes. (**a**) Linear scanning *J*–*V* curves in 1 m NaOH under 100 $mW{\cdot}cm^{-2}$ illumination; (**b**) Calculated charge separation efficiency, η_{sep}, and minority charge carrier injection efficiency, η_{inj}. Reprinted with permission from ref. [42]. Copyright 2018. Wiley.

Table 1. The hole diffusion length of different materials.

Materials	Hole Diffusion Length	Ref.
$BiVO_4$	100 nm	[43]
α-Fe_2O_3	2–4 nm	[44]
TiO_2	70 nm	[45]
WO_3	150 nm	[46]

3.3. Heterojunction

A heterojunction comprises, but is not limited to, two materials, whereby electron–hole pairs are produced by one or more semiconductor photocatalysts and then transfer to the other material, which facilitates the space charge separation [47]. The two materials should meet some requirements. Taking a photoanode as an example, the valence band of A is more positive than B; at the same time, the conduction band of photocatalyst B should be more negative than A. This would facilitate the electron and hole transfer from one to the other (Figure 15). A lot of work has reported the heterojunction for enhanced PEC performance, such as WO_3/$BiVO_4$ [48,49], Cu_2O/g-C_3N_4 [50], Cu_2O/TiO_2, p-Cu_2O/n-TaON [51]. It is also found that heterojunction can be formed between different facets of the same crystal, e.g., $BiVO_4$ (010) and $BiVO_4$ (110) surfaces. The electrons and holes can accumulate on different surfaces of $BiVO_4$ (Figure 16) [52], which causes the space separation of

electron–hole. Wang et al. found improved hydrogen production in a TiO_2 photocatalyst by forming {001}-{010} "quasi" heterojunctions [53]. Another case of heterojunctions is α-Fe_2O_3-TiO_2 heterojunction. Holes generated in TiO_2 will be transferred to α-Fe_2O_3 with electrons preferentially accumulating in TiO_2 at the same time. Under specific conditions, hybrid composites such as Fe_2TiO_5, Fe_3TiO_4, and $FeTiO_3$ form at the interface between hematite and titania that, despite some controversial results, exhibit remarkable performances as photoanode materials in PEC devices [54].

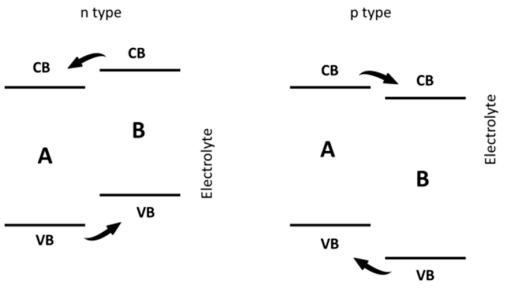

Figure 15. The band structure for the different heterojunctions. CB stands for conduct band and VB stands for valance band.

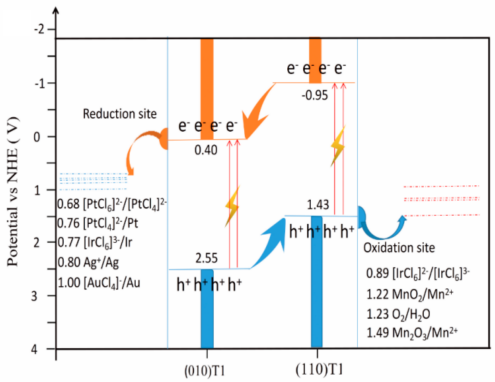

Figure 16. Schematic diagram of the heterojunction on between $BiVO_4$ (010) and $BiVO_4$ (110) surfaces. Reprinted with permission from ref. [52]. Copyright 2018. American Chemical Society.

3.4. Internal Electric Field to Improve the Charge Separation

Recent studies indicate that the internal electric field in a photocatalyst can improve the charge separation [55]. The internal electric field provides a driving force for the separation of photoinduced charge carriers. Ferroelectric materials are a big family for having internal electric field due to their spontaneous electric polarization property among various photocatalytic materials. The spontaneous polarization in ferroelectric materials are due to the noncentrosymmetric property and the polarization occurs because the positive and negative charges have different centers of symmetry [56]. Perovskite oxides (ABO_3) are among the most extensively studied ferroelectrics, such as $BaTiO_3$ [57] and $BiFeO_3$ [58]. Rohrer et al. found that $Ba_xSr_{1-x}TiO_3$ solid solution by replacing Ba with Sr can enlarge the space-charge region and improve the activity [59]. Zhang et al. also found that incorporation of carbon into the Bi_3O_4Cl lattice can increase internal electric field to boost bulk charge separation [60]. Hao et al. found that double perovskite ferroelectric $Bi_2FeMo_xNi_{1-x}O_6$ thin films also possess strong ferroelectric self-polarization, which has played a crucial part in improving the photovoltaic effect [61]. Another case of charge separation is α-Fe_2O_3-TiO_2 heterojunction. Some research works found that the Fe_2O_3-TiO_2 heterojunction showed enhancement in the photocurrent [62,63]. However, somehow it is not consistent with our general understanding on the heterojunction, because hematite has a more positive conduction band potential than TiO_2, which prohibits the electron transfer from hematite to

TiO_2. Further study shows that this kind of heterojunction is through iron titanates (e.g., Fe_2TiO_5, Fe_3TiO_4, and $FeTiO_3$) formed at the interface [54].

4. Strategies to Enhance the Surface Charge Injection

4.1. Catalyst Loading

In PEC water splitting, the catalyst loading play three vital roles for improving both the activity and reliability: (1) to reduce the overpotential or activation energy; (2) to assist charge separation at the semiconductor/electrolyte interface; (3) to suppress the photocorrosion and improve the durability of the working device [64]. Transition metal or transition metal oxides are usually used as catalyst loading to achieve a higher activity and decent reaction rates [65]. Recently, many (Fe, Co, Ni)-based catalyst loading have been widely investigated. For example, cobalt phosphate (CoPi) is the star cocatalyst to lower the overpotential and enhance the performance of water oxidation (Figure 17) [66]. Hydro-oxides are also one kind of effective catalyst loading, such as FeOOH, NiOOH, and CoOOH [67,68]. Kim et al. employed FeOOH/NiOOH dual-layer catalyst loading and achieved maximum ABPE of 1.75% due to reduction of the surface recombination [40]. Zhang et al. extended the catalyst loading to metal organic framework (MOF) materials, through applying in situ synthesized poly[-Co_2(benzimidazole)$_4$] nanoparticles on the surface of $BiVO_4$ to boost surface reaction kinetics (Figure 18) [69]. In this respect, the bilayered Ni-FeOOH oxygen evolution catalyst layer has been reported as the best catalysts for $BiVO_4$ to date [70].

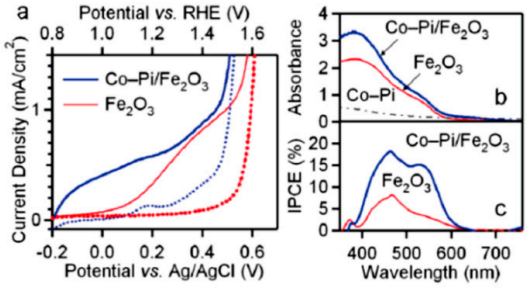

Figure 17. (**a**) Dark (dashed) and photocurrent (solid) densities for Fe_2O_3 (red) and Co–Pi/Fe_2O_3 (blue) photoanodes, collected using simulated AM 1.5 illumination (1 sun, backside) at a scan rate of 50 mV·s^{-1}; (**b**) Electronic absorption and (**c**) IPCE spectra for Fe_2O_3 and Co–Pi/Fe_2O_3 at 1.23 and 1 V vs. RHE, respectively. The absorption spectrum of Co–Pi on FTO without Fe_2O_3 is included in (**b**), but no photocurrent was detected for these anodes. Reprinted with permission from ref. [66]. Copyright 2018. American Chemical Society.

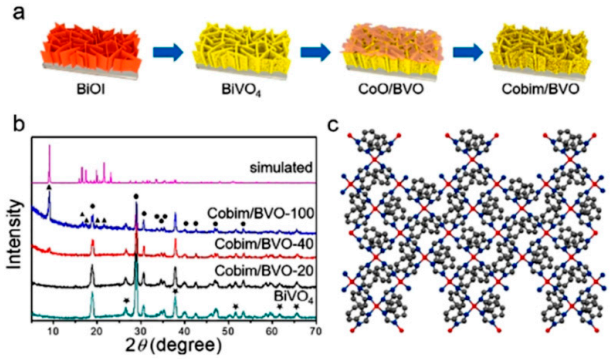

Figure 18. (**a**) Synthesis process of [Co_2(bim)$_4$]-modified $BiVO_4$ photoanodes; (**b**) XRD patterns of $BiVO_4$, Cobim/BiVO-20, Cobim/BiVO-40, Cobim/BiVO-100, and simulated [[Co_2(bim)$_4$], where the symbols asterisk, dot, and triangle correspond to the peaks from FTO, $BiVO_4$, and [Co_2(bim)$_4$], respectively; (**c**) Crystal structure of [Co_2(bim)$_4$], where gray, blue, and red balls represent carbon, nitrogen, and cobalt, respectively. Reprinted with permission from ref. [69]. Copyright 2018. American Chemical Society.

4.2. Surface Treatment and Surface Passivation

Point defects are usually found on the surface of photoelectrode. In some cases, defects play a positive role in the surface catalysis. However, in some other cases, defects serve as recombination centers. Thus, it is important to suppress the recombination on these surface centers. Recently, it was found that the surface treatment can improve the PEC performance. The mechanism for surface treatment and surface passivation is illustrated in Figure 19 [71].

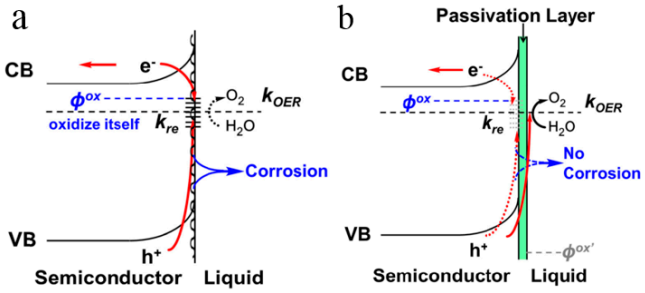

Figure 19. Band structure of an n-type semiconductor photoelectrode experiencing corrosion (**a**) when contacting an aqueous electrolyte; (**b**) with passivation layer without corrosion. ϕ_{ox} is the corrosion potential of the n-type semiconductor; and ϕ_{red} is the corrosion potential of the p-type semiconductor. Corrosion may reduce the light absorption and/or generate more surface defect states. Reprinted with permission from ref. [71] Copyright 2014. The Royal Society of Chemistry.

Surface defect states will lead to high charge recombination rate and water oxidation with low efficiency, caused by the photogenerated holes. Surface passivation and treatment can passivate defect states, forcefully suppressing surface recombination for improving water oxidation efficiency. For example, Luo et al. found that electrochemical cyclic voltammetry surface pretreatment on Mo-doped $BiVO_4$ can greatly enhances the photocurrent of Mo-doped $BiVO_4$ [72]. This is mainly because the pretreatment that can remove the surface recombination center MoO_x which is segregated during the preparation of the photoelectrode. After the preprocessing, MoO_x on the surface is dissolved into the electrolyte (Figure 20).

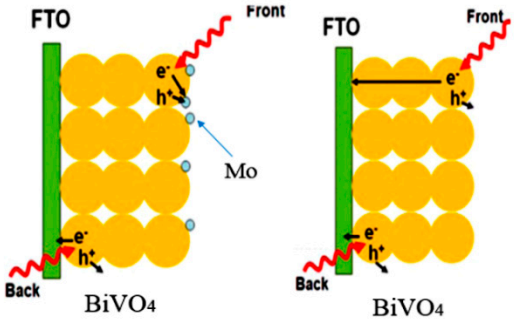

Figure 20. Transfer of photogenerated electrons in Mo-doped $BiVO_4$ photoelectrodes illuminated from the front-side and the back-side. Reprinted with permission from ref. [72]. Copyright 2018. American Chemical Society.

Further, Wang et al. found that the electrochemical treatment is not only suitable for doped $BiVO_4$, but also applicable to pristine $BiVO_4$ and other materials, such as TiO_2, Fe_2O_3 [73]. Besides the surface treatment, a thin passivation layer is also proved to be effective to enhance the surface catalysis. Originally, passivation layers were applied to semiconductor photoelectrodes to improve their photochemical or chemical stability. It was reported that even an extremely thin layer on the photoelectrodes can change the surface properties [74]. Hisatomi investigated the oxide surface layer on the onset potential of hematite photoanode, such as Al_2O_3, Ga_2O_3, and In_2O_3, which can greatly weaken the original potential

for oxidation of water [75]. Formal et al. covered an extremely thin layer (0.1 to 2 nm) of alumina on nanostructured hematite photoanodes. The photocurrent was shifted cathodically by as much as 100 mV. Further investigation found that the cathodic shift is owing to the passivation of surface trapping states caused by the Al_2O_3 overlayer [76]. Besides, IrO_2 and CoO_x thin layers on TaON photoanodes were found to improve the durability by reducing the self-oxidation of the electrode [77,78]. In general, a suitable structure of the passivation layer for photoelectrodes can either improve the reaction kinetics, or increase the chemical or physical protection against corrosion, or both.

4.3. Active Sites

The chemical reactions for water splitting occur on the electrode surface through its active sites. The active sites, therefore, affect the performance of the surface catalysis. The low catalytic activities are mainly attributed to the relatively lower activity and smaller number of reactive sites. The activity of active sites can be reflected by the overpotential at the anode. Experimentally, it might be extremely challenging to identify the atomic surface active sites. Therefore, calculations using density functional theory (DFT) become important to reveal the overpotential at different sites, as well as to understand the atomic/molecular mechanism. There are some methods to calculate the overpotential based on different reaction process [79,80]. The well acceptable reaction process is the four intermediate steps reaction path, as shown in R3 to R6.

The overpotential tends to zero if $\Delta G^{\theta}_{R3} = \Delta G^{\theta}_{R4} = \Delta G^{\theta}_{R5} = \Delta G^{\theta}_{R6} = 1.23$ eV and this would define the ideal catalyst, as shown in Figure 21 [81].

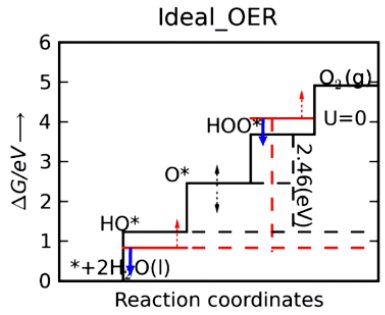

Figure 21. The free energy diagram for the OER ideal catalyst. The black continuous line is the OER ideal catalyst, where the over-potential is 0 eV because all free energies of the intermediate steps equal to 1.23 V. Red lines show the actual HOO* and HO* levels for the catalysts, which have to be moved down and up, respectively, in order to reduce the over-potential. Unfortunately, a metal oxide catalyst usually changes these two levels in the same direction, as indicated by the red (move up) and blue arrows (move down). O* level is positioned between the HOO* and HO* level. Reprinted with permission from ref. [81]. Copyright 2012. The Royal Society of Chemistry.

Until now, the atomic level interaction between catalytic activity and active sites is still an outstanding problem, owing to the large difference between idealized models and real catalysts. Thus, it is necessary to identify the pivotal factors that influence the activity of reactive sites, in order to promote the catalytic properties. It is generally considered that the low coordinated steps, edges, terraces, kinks, and/or corner atoms are often the favorable catalytic reaction sites [82,83]. For example, Sun et al. suggested that the low-coordinated Co^{3+} atoms of porous atomically-thick Co_3O_4 sheets serve as the catalytically active sites [84]. Currently, there are no quantitative models to describe the relationship between the coordinated number and activity. The main reason for this difficulty is that there might be other key parameters that have not been separately verified. For example, some results show that the surface state of the atom and position of neighbor atom will greatly affect the activity of the reactive sites. Hu et al. found that oxygen vacancy in $BiVO_4$ will induce more active sites on a $BiVO_4$ surface, which makes the vacancy sites active for water oxidation (Figure 22) [85]. Similarly, a Ti 3*d* defect state in the band gap of titania also plays an important role in the surface catalysis of

defect contained TiO_2 [86]. Zhao et al. also revealed that W doping and W–Ti codoping into $BiVO_4$ have led to more active sites on the surface and reduced charge transfer resistance (Figure 23) [87,88]. Theoretical calculation revealed that Ti sites become active after the codoping.

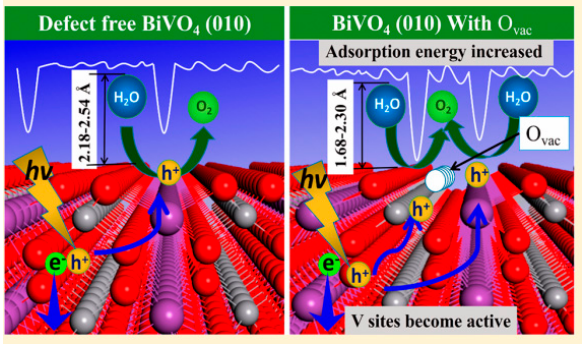

Figure 22. PEC water splitting process on a $BiVO_4$ (010) facet with or without O_{vac}. O_{vac} will greatly affect the adsorption energy. Reprinted with permission from ref. [85]. Copyright 2017. American Chemical Society.

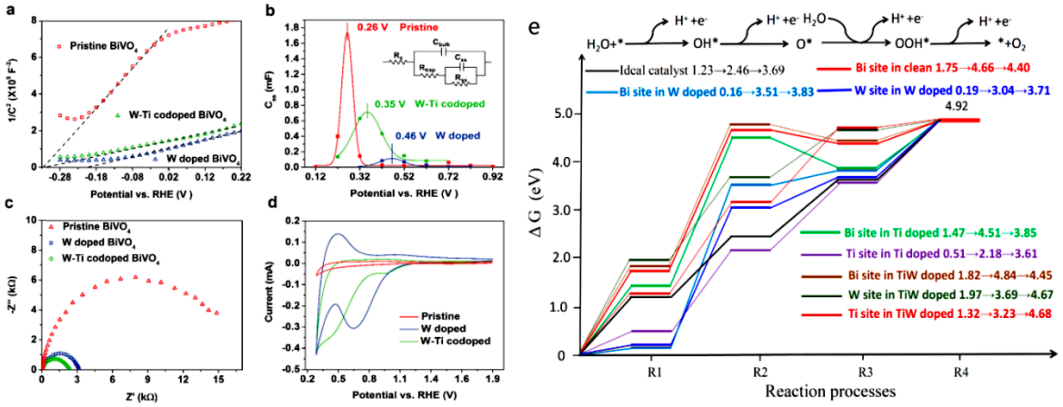

Figure 23. Electrochemistry results in 0.5 M Na_2SO_4 aqueous solution under 1.5 G illumination (**a**) Mott-Schottky plots of pristine, W doped $BiVO_4$ and W–Ti codoped $BiVO_4$ at the frequency of 1 kHz; (**b**) C_{ss} determined from EIS (rectangle points). Inset is the equivalent circuits employed to fit the experimental EIS data; (**c**) EIS of pristine, W doped, and W–Ti codoped $BiVO_4$ photoelectrodes at the applied potential of 1.23 V RHE; (**d**) Cyclic voltammetry scan of pristine, W doped and W–Ti codoped $BiVO_4$ in the dark at a scan rate of 100 $mV{\cdot}s^{-1}$ after holding the electrode at the potential of 1.8 V RHE for 120 s; (**e**) Free-energy profiles of OER on different sites of $BiVO_4$ surfaces. Reprinted with permission from ref. [88]. Copyright 2018. The Royal Society of Chemistry.

5. Conclusions and Outlook

In this review, we have highlighted the latest studies directed at developing metal oxide-based photoanodes, including $BiVO_4$, α-Fe_2O_3, TiO_2, and WO_3 nanostructures. We have summarized the strategies to enhance the light absorption, charge separation, and surface charge injection of this class of n-type semiconductor oxide materials. Although great achievements have been obtained, significant challenges remain before commercially viable solar-driven water splitting can be realized. Among them, one challenge is to balance the contributions from factors affecting light absorption, charge separation, and charge injection. Sometimes, their contributions contradict each other; e.g., a thicker layer increases absorption efficiency, but reduces the charge separation efficiency due to a longer distance to be travelled by the charge carrier. Another challenge lies with the lack of thorough understanding of the effect of the surface-state, due to the complex roles it plays in the water splitting process. Surface states may affect the amount of stored charges, act as surface recombination centers, and pin the Fermi-level. Most of the existing models can only explain one of these potential effects

and there is no commonly used model to describe the full impact of surface state. A big challenge is to combine all the advantages and improve the overall efficiency for water splitting. Usually, it is inevitable to introduce some other problems when improving one factor. For example, nanostructuring is mostly employed to enhance the charge separation and light absorption; however, more surface states will be formed which sometimes are unfavorable to the interfacial charge injection. Thus, catalyst loading is required to passivate the surface states. Then, the challenge becomes finding a suitable catalyst loading to passivate and to control its thickness through a proper deposition technology.

Recently, researchers are focusing on the formation of ultrathin layers of cocatalyst on the surface, which will provide very efficient charge injection while avoiding the recombination in the surface layer and at the interface. However, it is very difficult to precisely control the formation of a uniform cover layer of the cocatalyst on the surface with reasonable cost of production. New low-cost processing technology and materials need to be developed. Another related issue is the stability and durability from the point of view of practical application. Newly developed materials should be coated with good adhesion while having good chemical and photochemical stability. More work is needed to build a more comprehensive model to guide the design and optimization of the electrode materials for solar water splitting.

Funding: This research was funded by Ministry of Education of Singapore (RG15/16), the National Natural Science Foundation of China (Nos. 21676216, 21576224) and China Postdoctoral Science Foundation (Nos. 2014M550507; 2015T81046).

Conflicts of Interest: The authors declare no conflict of interest.

References

1. van de Krol, R.; Grätzel, M. *Photoelectrochemical Hydrogen Production*; Springer: Berlin, Germany, 2012; pp. 13–69.
2. Inoue, H.; Shimada, T.; Kou, Y.; Nabetani, Y.; Masui, D.; Takagi, S.; Tachibana, H. The water oxidation bottleneck in artificial photosynthesis: How can we get through it? an alternative route involving a two-electron process. *ChemSusChem* **2011**, *4*, 173–179. [CrossRef]
3. Fujishima, A.; Honda, K. Electrochemical photolysis of water at a semiconductor electrode. *Nature* **1972**, *238*, 37–38. [CrossRef] [PubMed]
4. Sivula, K.; Van De Krol, R. Semiconducting materials for photoelectrochemical energy conversion. *Nat. Rev. Mater.* **2016**, *1*, 15010. [CrossRef]
5. Li, Z.; Luo, W.; Zhang, M.; Feng, J.; Zou, Z. Photoelectrochemical cells for solar hydrogen production: Current state of promising photoelectrodes, methods to improve their properties, and outlook. *Energy Environ. Sci.* **2013**, *6*, 347–370. [CrossRef]
6. Zhou, Y.; Zhang, L.; Lin, L.; Wygant, B.R.; Liu, Y.; Zhu, Y.; Zheng, Y.; Mullins, C.B.; Zhao, Y.; Zhang, X. Highly efficient photoelectrochemical water splitting from hierarchical WO_3/$BiVO_4$ nanoporous sphere arrays. *Nano Lett.* **2017**, *17*, 8012–8017. [CrossRef] [PubMed]
7. Zhao, J.; Wang, A.; Green, M.A.; Ferrazza, F. 19.8% efficient "honeycomb" textured multicrystalline and 24.4% monocrystalline silicon solar cells. *Appl. Phys. Lett.* **1998**, *73*, 1991–1993. [CrossRef]
8. Zhao, X.; Chen, Z. Enhanced photoelectrochemical water splitting performance using morphology-controlled $BiVO_4$ with W doping. *Beilstein J. Nanotechnol.* **2017**, *8*, 2640–2647. [CrossRef] [PubMed]
9. Qiu, Y.; Liu, W.; Chen, W.; Zhou, G.; Hsu, P.-C.; Zhang, R.; Liang, Z.; Fan, S.; Zhang, Y.; Cui, Y. Efficient solar-driven water splitting by nanocone $BiVO_4$-perovskite tandem cells. *Sci. Adv.* **2016**, *2*, e1501764. [CrossRef]
10. Feng, X.; Shankar, K.; Varghese, O.K.; Paulose, M.; Latempa, T.J.; Grimes, C.A. Vertically aligned single crystal TiO_2 nanowire arrays grown directly on transparent conducting oxide coated glass: Synthesis details and applications. *Nano Lett.* **2008**, *8*, 3781–3786. [CrossRef] [PubMed]
11. Lou, S.N.; Amal, R.; Scott, J.; Ng, Y.H. Concentration-mediated band gap reduction of Bi_2MoO_6 photoanodes prepared by Bi^{3+} cation insertions into anodized MoO_3 thin films: Structural, optical, and photoelectrochemical properties. *ACS Appl. Energy Mater.* **2018**, *1*, 3955–3964. [CrossRef]
12. Mai, L.; Yang, F.; Zhao, Y.; Xu, X.; Xu, L.; Hu, B.; Luo, Y.; Liu, H. Molybdenum oxide nanowires: Synthesis & properties. *Mater. Today* **2011**, *14*, 346–353. [CrossRef]

13. Lou, S.N.; Ng, Y.H.; Ng, C.; Scott, J.; Amal, R. Harvesting, storing and utilising solar energy using MoO_3: Modulating structural distortion through pH adjustment. *ChemSusChem* **2014**, *7*, 1934–1941. [CrossRef]
14. Asahi, R.; Morikawa, T.; Irie, H.; Ohwaki, T. Nitrogen-doped titanium dioxide as visible-light-sensitive photocatalyst: Designs, developments, and prospects. *Chem. Rev.* **2014**, *114*, 9824–9852. [CrossRef]
15. Liu, G.; Yin, L.C.; Wang, J.; Niu, P.; Zhen, C.; Xie, Y.; Cheng, H.M. A red anatase TiO_2 photocatalyst for solar energy conversion. *Energy Environ. Sci.* **2012**, *5*, 9603–9610. [CrossRef]
16. Xie, J.; Zhang, J.; Li, S.; Grote, F.; Zhang, X.; Zhang, H.; Wang, R.; Lei, Y.; Pan, B.; Xie, Y. Controllable disorder engineering in oxygen-incorporated MoS_2 ultrathin nanosheets for efficient hydrogen evolution. *J. Am. Chem. Soc.* **2013**, *135*, 17881–17888. [CrossRef] [PubMed]
17. Morikawa, T.; Saeki, S.; Suzuki, T.; Kajino, T.; Motohiro, T. Dual functional modification by N doping of Ta_2O_5: P-type conduction in visible-light-activated N-doped Ta_2O_5. *Appl. Phys. Lett.* **2010**, *96*, 142111. [CrossRef]
18. Maeda, K.; Takata, T.; Hara, M.; Saito, N.; Inoue, Y.; Kobayashi, H.; Domen, K. GaN: ZnO solid solution as a photocatalyst for visible-light-driven overall water splitting. *J. Am. Chem. Soc.* **2005**, *127*, 8286–8287. [CrossRef] [PubMed]
19. Chen, X.; Liu, L.; Yu, P.Y.; Mao, S.S. Increasing solar absorption for photocatalysis with black hydrogenated titanium dioxide nanocrystals. *Science* **2011**, *331*, 746–750. [CrossRef]
20. Naldoni, A.; Altomare, M.; Zoppellaro, G.; Liu, N.; Kment, Š.; Zbořil, R.; Schmuki, P. Photocatalysis with reduced TiO_2: From black TiO_2 to cocatalyst-free gydrogen production. *ACS Catal.* **2019**, *9*, 345–364. [CrossRef] [PubMed]
21. Cui, H.; Zhao, W.; Yang, C.; Yin, H.; Lin, T.; Shan, Y.; Xie, Y.; Gu, H.; Huang, F. Black TiO_2 nanotube arrays for high-efficiency photoelectrochemical water-splitting. *J. Mater. Chem. A* **2014**, *2*, 8612–8616. [CrossRef]
22. Wang, S.; Chen, P.; Bai, Y.; Yun, J.H.; Liu, G.; Wan, L. New $BiVO_4$ dual photoanodes with enriched oxygen vacancies for efficient solar-driven water splitting. *Adv. Mater.* **2018**, *30*, 1800486. [CrossRef] [PubMed]
23. Kim, J.H.; Jang, J.W.; Jo, Y.H.; Abdi, F.F.; Lee, Y.H.; Van De Krol, R.; Lee, J.S. Hetero-type dual photoanodes for unbiased solar water splitting with extended light harvesting. *Nat. Commun.* **2016**, *7*, 13380. [CrossRef] [PubMed]
24. Mayer, M.T.; Du, C.; Wang, D. Hematite/Si nanowire dual-absorber system for photoelectrochemical water splitting at low applied potentials. *J. Am. Chem. Soc.* **2012**, *134*, 12406–12409. [CrossRef] [PubMed]
25. Brillet, J.; Yum, J.-H.; Cornuz, M.; Hisatomi, T.; Solarska, R.; Augustynski, J.; Graetzel, M.; Sivula, K. Highly efficient water splitting by a dual-absorber tandem cell. *Nat. Photonics* **2012**, *6*, 824. [CrossRef]
26. Chang, X.; Wang, T.; Zhang, P.; Zhang, J.; Li, A.; Gong, J. Enhanced surface reaction kinetics and charge separation of p–n heterojunction $Co_3O_4/BiVO_4$ photoanodes. *J. Am. Chem. Soc.* **2015**, *137*, 8356–8359. [CrossRef] [PubMed]
27. Ye, K.; Wang, Z.; Gu, J.; Xiao, S.; Yuan, Y.; Zhu, Y.; Zhang, Y.; Mai, W.; Yang, S. Carbon quantum dots as a visible light sensitizer to significantly increase the solar water splitting performance of bismuth vanadate photoanodes. *Energy Environ. Sci.* **2017**, *10*, 772–779. [CrossRef]
28. Kim, J.K.; Shi, X.; Jeong, M.J.; Park, J.; Han, H.S.; Kim, S.H.; Guo, Y.; Heinz, T.F.; Fan, S.; Lee, C.L.; et al. Enhancing Mo:$BiVO_4$ Solar Water Splitting with Patterned Au Nanospheres by Plasmon-Induced Energy Transfer. *Adv. Energy Mater.* **2018**, *8*, 1701765. [CrossRef]
29. Thimsen, E.; Formal, F.L.; Grätzel, M.; Warren, S.C. Influence of plasmonic Au nanoparticles on the photoactivity of Fe_2O_3 electrodes for water splitting. *Nano Lett.* **2011**, *11*, 35–43. [CrossRef]
30. Mascaretti, L.; Dutta, A.; Kment, Š.; Shalaev, V.M.; Boltasseva, A.; Zbořil, R.; Naldoni, A. Plasmon-enhanced photoelectrochemical water splitting for efficient renewable energy storage. *Adv. Mater.* **2019**, 1805513. [CrossRef]
31. Zhao, X.; Feng, J.; Chen, S.; Huang, Y.; Sum, T.C.; Chen, Z. New insight into the roles of oxygen vacancies in hematite for solar water splitting. *Phys. Chem. Chem. Phys.* **2017**, *19*, 1074–1082. [CrossRef]
32. Luo, W.; Yang, Z.; Li, Z.; Zhang, J.; Liu, J.; Zhao, Z.; Wang, Z.; Yan, S.; Yu, T.; Zou, Z. Solar hydrogen generation from seawater with a modified $BiVO_4$ photoanode. *Energy Environ. Sci.* **2011**, *4*, 4046–4051. [CrossRef]
33. Berglund, S.P.; Rettie, A.J.E.; Hoang, S.; Mullins, C.B. Incorporation of Mo and W into nanostructured $BiVO_4$ films for efficient photoelectrochemical water oxidation. *Phys. Chem. Chem. Phys.* **2012**, *14*, 7065–7075. [CrossRef]

34. Guo, Y.; Zhang, N.; Wang, X.; Qian, Q.; Zhang, S.; Li, Z.; Zou, Z. A facile spray pyrolysis method to prepare Ti-doped $ZnFe_2O_4$ for boosting photoelectrochemical water splitting. *J. Mater. Chem. A* **2017**, *5*, 7571–7577. [CrossRef]
35. Lumley, M.A.; Choi, K.S. Investigation of pristine and (Mo, W)-doped $Cu_{11}V_6O_{26}$ for use as photoanodes for solar water splitting. *Chem. Mater.* **2017**, *29*, 9472–9479. [CrossRef]
36. Jo, W.J.; Jang, J.W.; Kong, K.; Kang, H.J.; Kim, J.Y.; Jun, H.; Parmar, K.P.S.; Lee, J.S. Phosphate doping into monoclinic $BiVO_4$ for enhanced photoelectrochemical water oxidation activity. *Angew. Chem. Int. Ed.* **2012**, *51*, 3147–3151. [CrossRef]
37. Yang, Z.; Chang, B.; Zou, J.; Qiao, J.; Gao, P.; Zeng, Y.; Li, H. Comparison between gradient-doping GaAs photocathode and uniform-doping GaAs photocathode. *Appl. Opt.* **2007**, *46*, 7035–7039. [CrossRef]
38. Abdi, F.F.; Han, L.; Smets, A.H.; Zeman, M.; Dam, B.; Van De Krol, R. A bismuth vanadate–cuprous oxide tandem cell for overall solar water splitting. *Nat. Commun.* **2013**, *4*, 2195. [CrossRef]
39. Krol, R.; Liang, Y.; Schoonman, J. Solar hydrogen production with nanostructured metal oxides. *J. Mater. Chem.* **2008**, *18*, 2311–2320. [CrossRef]
40. Kim, T.W.; Choi, K.-S. Nanoporous $BiVO_4$ photoanodes with dual-layer oxygen evolution catalysts for solar water splitting. *Science* **2014**, *343*, 990–994. [CrossRef]
41. Zhao, X.; Luo, W.; Feng, J.; Li, M.; Li, Z.; Yu, T.; Zou, Z. Quantitative analysis and visualized evidence for high charge separation efficiency in a solid-liquid bulk heterojunction. *Adv. Energy Mater.* **2014**, *4*, 1301785. [CrossRef]
42. Zhu, X.; Guijarro, N.; Liu, Y.; Schouwink, P.; Wells, R.A.; Formal, F.L.; Sun, S.; Gao, C.; Sivula, K. Spinel structural disorder influences solar-water-splitting performance of $ZnFe_2O_4$ nanorod photoanodes. *Adv. Mater.* **2018**, *30*, 1801612. [CrossRef]
43. Iwase, A.; Yoshino, S.; Takayama, T.; Ng, Y.H.; Amal, R.; Kudo, A. Water splitting and CO_2 reduction under visible light irradiation using Z-Scheme systems consisting of metal sulfides, CoO_x-loaded $BiVO_4$, and a reduced graphene oxide electron mediator. *J. Am. Chem. Soc.* **2016**, *138*, 10260–10264. [CrossRef]
44. Booshehri, A.Y.; Goh, S.C.; Hong, J.D.; Jiang, R.; Xu, R. Effect of depositing silver nanoparticles on $BiVO_4$ in enhancing visible light photocatalytic inactivation of bacteria in water. *J. Mater. Chem. A* **2014**, *2*, 6209–6217. [CrossRef]
45. Zhang, Z.; Wang, P. Optimization of photoelectrochemical water splitting performance on hierarchicalTiO_2 nanotube arrays. *Energy Environ. Sci.* **2012**, *5*, 6506–6512. [CrossRef]
46. Butler, M.A. Photoelectrolysis and physical properties of the semiconducting electrode WO_2. *J. Appl. Phys.* **1977**, *48*, 1914–1920. [CrossRef]
47. Moniz, S.J.; Shevlin, S.A.; Martin, D.J.; Guo, Z.-X.; Tang, J. Visible-light driven heterojunction photocatalysts for water splitting–a critical review. *Energy Environ. Sci.* **2015**, *8*, 731–759. [CrossRef]
48. Su, J.; Guo, L.; Bao, N.; Grimes, C.A. Nanostructured WO_3/$BiVO_4$ heterojunction films for efficient photoelectrochemical water splitting. *Nano Lett.* **2011**, *11*, 1928–1933. [CrossRef]
49. Rao, P.M.; Cai, L.; Liu, C.; Cho, I.S.; Lee, C.H.; Weisse, J.M.; Yang, P.; Zheng, X. Simultaneously efficient light absorption and charge separation in WO_3/$BiVO_4$ core/shell nanowire photoanode for photoelectrochemical water oxidation. *Nano Lett.* **2014**, *14*, 1099–1105. [CrossRef]
50. Zhang, S.; Yan, J.; Yang, S.; Xu, Y.; Cai, X.; Li, X.; Zhang, X.; Peng, F.; Fang, Y. Electrodeposition of Cu_2O/g-C_3N_4 heterojunction film on an FTO substrate for enhancing visible light photoelectrochemical water splitting. *Chin. J. Catal.* **2017**, *38*, 365–371. [CrossRef]
51. Hou, J.; Yang, C.; Cheng, H.; Jiao, S.; Takeda, O.; Zhu, H. High-performance p-Cu_2O/n-TaON heterojunction nanorod photoanodes passivated with an ultrathin carbon sheath for photoelectrochemical water splitting. *Energy Environ. Sci.* **2014**, *7*, 3758–3768. [CrossRef]
52. Hu, J.; Chen, W.; Zhao, X.; Su, H.; Chen, Z. Anisotropic electronic characteristics, adsorption, and stability of low-index $BiVO_4$ surfaces for photoelectrochemical applications. *ACS Appl. Mater. Interfaces* **2018**, *10*, 5475–5484. [CrossRef]
53. Wang, D.; Kanhere, P.; Li, M.; Tay, Q.; Tang, Y.; Huang, Y.; Sum, T.C.; Mathews, N.; Sritharan, T.; Chen, Z. Improving Photocatalytic H_2 Evolution of TiO_2 via Formation of {001}−{010} Quasi-Heterojunctions. *J. Phys. Chem. C* **2013**, *117*, 22894–22902. [CrossRef]

54. Kment, S.; Riboni, F.; Pausova, S.; Wang, L.; Wang, L.; Han, H.; Hubicka, Z.; Krysa, J.; Schmuki, P.; Zboril, R. Photoanodes based on TiO_2 and α-Fe_2O_3 for solar water splitting—Superior role of 1D nanoarchitectures and of combined heterostructures. *Chem. Soc. Rev.* **2017**, *46*, 3716–3769. [CrossRef]
55. Huang, X.; Wang, K.; Wang, Y.; Wang, B.; Zhang, L.; Gao, F.; Zhao, Y.; Feng, W.; Zhang, S.; Liu, P. Enhanced charge carrier separation to improve hydrogen production efficiency by ferroelectric spontaneous polarization electric field. *Appl. Catal. B-Environ.* **2018**, *227*, 322–329. [CrossRef]
56. Li, L.; Salvador, P.A.; Rohrer, G.S. Photocatalysts with internal electric fields. *Nanoscale* **2014**, *6*, 24–42. [CrossRef]
57. Giocondi, J.L.; Rohrer, G.S. The influence of the dipolar field effect on the photochemical reactivity of $Sr_2Nb_2O_7$ and $BaTiO_3$ microcrystals. *Top. Catal.* **2008**, *49*, 18–23. [CrossRef]
58. Schultz, A.M.; Zhang, Y.; Salvador, P.A.; Rohrer, G.S. Effect of crystal and domain orientation on the visible-light photochemical reduction of Ag on $BiFeO_3$. *ACS Appl. Mater. Interfaces* **2011**, *3*, 1562–1567. [CrossRef]
59. Bhardwaj, A.; Burbure, N.V.; Gamalski, A.; Rohrer, G.S. Composition dependence of the photochemical reduction of Ag by $Ba_{1-x}Sr_xTiO_3$. *Chem. Mater.* **2010**, *22*, 3527–3534. [CrossRef]
60. Li, J.; Cai, L.; Shang, J.; Yu, Y.; Zhang, L. Giant enhancement of internal electric field boosting bulk charge separation for photocatalysis. *Adv. Mater.* **2016**, *28*, 4059–4064. [CrossRef]
61. Cui, X.; Li, Y.; Sun, N.; Dua, J.; Lia, X.; Yang, H.; Hao, X. Double perovskite $Bi_2FeMo_xNi_{1-x}O_6$ thin films: Novel ferroelectric photovoltaic materials with narrow bandgap and enhanced photovoltaic performance. *Sol. Energy Mater. Sol. C* **2018**, *187*, 9–14. [CrossRef]
62. Han, H.; Riboni, F.; Karlicky, F.; Kment, S.; Goswami, A.; Sudhagar, P.; Yoo, J.; Wang, L.; Tomanec, O.; Petr, M.; et al. α-Fe_2O_3/TiO_2 3D hierarchical nanostructures for enhanced photoelectrochemical water splitting. *Nanoscale* **2017**, *9*, 134–142. [CrossRef] [PubMed]
63. Jeon, T.H.; Choi, W.; Park, H. Photoelectrochemical and photocatalytic behaviors of hematite-decorated Titania nanotube arrays: Energy level mismatch versus surface specific reactivity. *J. Phys. Chem. C* **2011**, *115*, 7134–7142. [CrossRef]
64. Ran, J.; Zhang, J.; Yu, J.; Jaroniec, M.; Qiao, S.Z. Earth-abundant cocatalysts for semiconductor-based photocatalytic water splitting. *Chem. Soc. Rev.* **2014**, *43*, 7787–7812. [CrossRef] [PubMed]
65. Maeda, K.; Domen, K. Photocatalytic water splitting: Recent progress and future challenges. *J. Phys. Chem. Lett.* **2010**, *1*, 2655–2661. [CrossRef]
66. Zhong, D.K.; Sun, J.; Inumaru, H.; Gamelin, D.R. Solar water oxidation by composite catalyst/α-Fe_2O_3 photoanodes. *J. Am. Chem. Soc.* **2009**, *131*, 6086–6087. [CrossRef] [PubMed]
67. Kim, T.W.; Ping, Y.; Galli, G.A.; Choi, K.S. Simultaneous enhancements in photon absorption and charge transport of bismuth vanadate photoanodes for solar water splitting. *Nat. Commun.* **2015**, *6*, 8769. [CrossRef] [PubMed]
68. Tang, F.; Cheng, W.; Su, H.; Zhao, X.; Liu, Q. Smoothing surface trapping states in 3D coral-like CoOOH-wrapped-$BiVO_4$ for efficient photoelectrochemical water oxidation. *ACS Appl. Mater. Interfaces* **2018**, *10*, 6228–6234. [CrossRef]
69. Zhang, W.; Li, R.; Zhao, X.; Chen, Z.; Law, A.W.K.; Zhou, K. A cobalt-based metal–organic framework as cocatalyst on $BiVO_4$ photoanode for enhanced photoelectrochemical water oxidation. *ChemSusChem* **2018**, *11*, 2710–2716. [CrossRef]
70. Shi, X.; Choi, I.Y.; Kan, Z.; Kwon, J.; Dong, Y.K.; Lee, J.K.; Sang, H.O.; Kim, J.K.; Park, J.H. Efficient photoelectrochemical hydrogen production from bismuth vanadate-decorated tungsten trioxide helix nanostructures. *Nat. Commun.* **2014**, *5*, 4775. [CrossRef]
71. Liu, R.; Zheng, Z.; Spurgeon, J.; Yang, X. Enhanced photoelectrochemical water-splitting performance of semiconductors by surface passivation layers. *Energy Environ. Sci.* **2014**, *7*, 2504–2517. [CrossRef]
72. Luo, W.; Li, Z.; Yu, T.; Zou, Z. Effects of surface electrochemical pretreatment on the photoelectrochemical performance of Mo-Doped $BiVO_4$. *J. Phys. Chem. C* **2012**, *116*, 5076–5081. [CrossRef]
73. Wang, S.; Chen, P.; Yun, J.H.; Hu, Y.; Wang, L. An electrochemically treated $BiVO_4$ photoanode for efficient photoelectrochemical water splitting. *Angew. Chem. Int. Ed.* **2017**, *56*, 8500–8504. [CrossRef]
74. Riha, S.C.; Klahr, B.M.; Tyo, E.C.; Seifert, S.; Vajda, S.; Pellin, M.J.; Hamann, T.W.; Martinson, A.B.F. Atomic layer deposition of a submonolayer catalyst for the enhanced photoelectrochemical performance of water oxidation with hematite. *ACS Nano* **2013**, *7*, 2396–2405. [CrossRef]

75. Hisatomi, T.; Le Formal, F.; Cornuz, M.; Brillet, J.; Tétreault, N.; Sivula, K.; Grätzel, M. Cathodic shift in onset potential of solar oxygen evolution on hematite by 13-group oxide overlayers. *Energy Environ. Sci.* **2011**, *4*, 2512–2515. [CrossRef]
76. Le Formal, F.; Tetreault, N.; Cornuz, M.; Moehl, T.; Gr€atzel, M.; Sivula, K. Passivating surface states on water splitting hematite photoanodes with alumina overlayers. *Chem. Sci.* **2011**, *2*, 737–743. [CrossRef]
77. Abe, R.; Higashi, M.; Domen, K. Facile fabrication of an efficient oxynitride TaON photoanode for overall water splitting into H_2 and O_2 under visible light irradiation. *J. Am. Chem. Soc.* **2010**, *132*, 11828–11829. [CrossRef]
78. Higashi, M.; Domen, K.; Abe, R. Highly stable water splitting on oxynitride TaON photoanode system under visible light irradiation. *J. Am. Chem. Soc.* **2012**, *134*, 6968–6971. [CrossRef]
79. Yang, J.; Wang, D.; Zhou, X.; Li, C. A theoretical study on the mechanism of photocatalytic oxygen evolution on $BiVO_4$ in aqueous solution. *Chem. Eur. J.* **2013**, *19*, 1320–1326. [CrossRef]
80. Zhao, Z.Y. Single water molecule adsorption and decomposition on the low-index stoichiometric rutile TiO_2 surfaces. *J. Phys. Chem. C* **2014**, *118*, 4287–4295. [CrossRef]
81. Valdés, Á.; Brillet, J.; Grätzel, M.; Gudmundsdóttir, H.; Hansen, H.A.; Jónsson, H.; Klüpfel, P.; Kroes, G.J.; Formal, F.L.; Man, I.C.; et al. Solar hydrogen production with semiconductor metal oxides: New directions in experiment and theory. *Phys. Chem. Chem. Phys.* **2012**, *14*, 49–70. [CrossRef]
82. Sun, Y.F.; Liu, Q.H.; Gao, S.; Cheng, H.; Lei, F.C.; Sun, Z.H.; Jiang, Y.; Su, H.B.; Wei, S.Q.; Xie, Y. Pits confined in ultrathin cerium (IV) oxide for studying catalytic centers in carbon monoxide oxidation. *Nat. Commun.* **2013**, *4*, 2899. [CrossRef]
83. Sun, Y.F.; Lei, F.C.; Gao, S.; Pan, B.C.; Zhou, J.F.; Xie, Y. Atomically thin tin dioxide sheets for efficient catalytic oxidation of carbon monoxide. *Angew. Chem. Int. Ed.* **2013**, *52*, 10569. [CrossRef]
84. Sun, Y.F.; Gao, S.; Lei, F.C.; Liu, J.W.; Liang, L.; Xie, Y. Atomically-thin non-layered cobalt oxide porous sheets for highly efficient oxygen-evolving electrocatalysts. *Chem. Sci.* **2014**, *5*, 3976–3982. [CrossRef]
85. Hu, J.; Zhao, X.; Chen, W.; Su, H.; Chen, Z. Theoretical insight into the mechanism of photoelectrochemical oxygen evolution reaction on $BiVO_4$ anode with oxygen vacancy. *J. Phys. Chem. C* **2017**, *121*, 18702–18709. [CrossRef]
86. Wendt, S.; Sprunger, P.T.; Lira, E.; Madsen, G.K.H.; Li, Z.; Hansen, J.O.; Matthiesen, J.; Blekinge-Rasmussen, A.; Lægsgaard, E.; Hammer, B.; Besenbacher, F. The role of interstitial sites in the Ti_3D defect state in the band gap of Titania. *Science* **2008**, *320*, 1755–1759. [CrossRef] [PubMed]
87. Zhao, X.; Hu, J.; Chen, S.; Chen, Z. An investigation on the role of W doping in $BiVO_4$ photoanodes used for solar water splitting. *Phys. Chem. Chem. Phys.* **2018**, *20*, 13637–13645. [CrossRef] [PubMed]
88. Zhao, X.; Hu, J.; Wu, B.; Banerjee, A.; Chakraborty, S.; Feng, J.; Zhao, Z.; Chen, S.; Ahuja, R.; Sum, T.C.; Chen, Z. Simultaneous enhancement in charge separation and onset potential for water oxidation in a $BiVO_4$ photoanode by W–Ti codoping. *J. Mater. Chem. A* **2018**, *6*, 16965–16974. [CrossRef]